Nonadiabatic Molecular Dynamics Simulation of Light-Induced Electron Transfer from an Anchored Molecular Electron Donor to a Semiconductor Acceptor†

William Stier and Oleg V. Prezhdo*

Department of Chemistry, University of Washington, Seattle, Washington 98195-1700

Received: November 19, 2001; In Final Form: February 21, 2002

A nonadiabatic molecular dynamics (MD) simulation of the photoinduced electron transfer (ET) from a molecular electron donor to the TiO_2 acceptor is reported. The system under study is typical of the dye sensitized semiconductor nanomaterials used in solar cell, photocatalysis, and photoelectrolysis applications. The electronic structure of the dye−semiconductor system and the adiabatic dynamics are simulated by ab initio MD, whereas the nonadiabatic effects are incorporated by the quantum-classical mean-field approach. A novel procedure separating the nonadiabatic and adiabatic ET pathways is proposed. The simulation provides a detailed picture of the ET process. For the specific system under study, ET occurs on a 30 fs time scale, in agreement with the ultrafast experimental data. Both adiabatic and nonadiabatic pathways for the ET are observed. The nonadiabatic transfer entirely dominates at short times and can occur due to strong localized avoided crossing as well as extended regions of weaker nonadiabatic coupling. Although the adiabatic ET contribution accumulates more slowly, it approaches that of the nonadiabatic ET pathway asymptotically. It follows from the simulation that the nonadiabatic ET rate expressions, such as the Fermi golden rule, can be rigorously applied only for the fastest 30% of the ET process. The electron acceptor states are formed by the d orbitals of Ti atoms of the semiconductor and are localized within the first three to four layers of the surface. About 20% of the acceptor state density is localized on a single Ti atom of the first surface layer. The simulation predicts a complex non-single-exponential time dependence of the ET process.

1. Introduction

Electron transfer (ET) at semiconductor surfaces drives important applications including photocatalysis, photoelectrolysis, solar cells, waste processing, and quantum confinement devices.[1−5] Solar cells of the Graetzel type[6,7] are based on dye-sensitized nanocrystalline semiconductor films, typically containing transition metal or organic dye molecules adsorbed to a highly porous nanocrystalline anatase titanium dioxide. The Graetzel cells are a potential alternative to the conventional photovoltaic devices. In recent years these cells have demonstrated a solar energy conversion efficiency that is greater than the industry average of 10%.[8−10] The potentially lower cost of manufacturing of the Graetzel cells relative to the traditional silicon-based solar cells makes them even more attractive.[9] Considerable research has been focused on the charge transfer (CT) dynamics of these cells.[10−12] The overall photon to current efficiency is determined by a number of factors, most importantly, by the relative yields and rates of electron injection, recombination, and decay of the excited state of the dye.[13] A fast electron transfer from the sensitizer dye to the semiconductor and a much slower back ET are required. Low photovoltage appears to be the major limiting factor in the applications of the Graetzel cells. The experimentally observed photovoltage is below the theoretical maximum, likely due to the competition between ET and charge recombination pathways.[9] Knowledge of the rates and mechanisms of these competing reactions are vital to the efficient improvement of the solar devices.[13]

The present theoretical work focuses on the recent experiments on the ultrafast electron injection into a titanium dioxide surface from an adsorbed sensitizer chromophore.[11,14−16] The reported data obtained with high temporal resolution reveal the electron injection to occur on the femtosecond time scale. However, the exact mechanism of the ultrafast injection of electrons from the sensitizer to TiO_2 remains unclear. Both adiabatic pathways involving strong coupling between the state of the chromophore and a conductance band state in the semiconductor and nonadiabatic mechanisms involving weak coupling from the excited state of the dye to a manifold of the semiconductor states have been proposed to explain the observed ultrafast ET.[11,17] It has been shown in some cases that no redistribution of the vibrational excitation energy occurs prior to ET,[18] making it difficult to invoke the traditional Marcus−Levich−Jorter−Gerischer[19−22] ET mechanism as well as the modern analytical and computational reaction rate theories.[23−32] The observed ultrafast interplay between the electronic and vibrational degrees of freedom makes the dye−semiconductor system ideal for a direct nonadiabatic molecular dynamics (MD) simulation,[33−45] where the electronic states and atomic coordinates are coupled and evolve in real time.

The femtosecond laser experiments of the ultrafast ET have been carried out with a variety of chromophores and substrates by several research groups throughout the world.[11,14−16] Anatase titanium dioxide with an absorbed Ru[NCS]bypy chromophore replenished from a liquid environment is among the most promising solar cell systems. A more rigorous characterization of this class of reactions has been achieved in experiments with a perylene dye in an ultrahigh vacuum environment and over a range of temperatures.[46] Isonicotinic acid is the chromophore in our simulation, Figure 1. This small chromophore is expected to exhibit the general behavior of the more complex molecules used in the experiments, whereas the reduced number of atoms

† Part of the special issue "John C. Tully Festschrift".

* Corresponding author. E-mail: prezhdo@u.washington.edu.

10.1021/jp014267b CCC: $22.00
Published on Web 07/17/2002

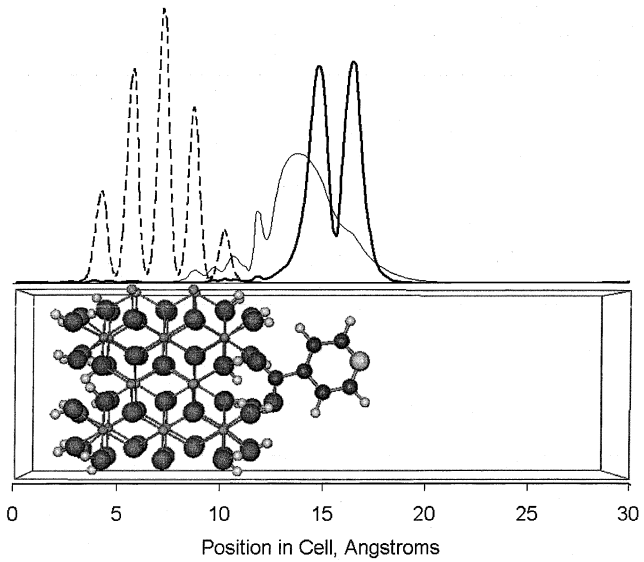

Figure 1. Simulation cell. The TiO_2 semiconductor surface with a covalently attached isonicotinic acid and a vacuum region of the cell are shown in the bottom. The top part depicts densities of a typical TiO_2 conductance band state (dashed line) and the first (dark solid line) and second (light solid line) excited states of the dye.

makes the simulation much easier to accomplish. Similar to perylene, the lower excited states of the model chromophore are localized in the conjugated π-system. As in the perylene chromophore, the acid group of the model chromophore provides the chemical bridge to the semiconductor surface. The model dye is evocative of the most often used sensitizing dye, Ru[NCS]bypy: Isonicotinic acid, also referred to as pyridine-4-carboxylic acid, is essentially half of a bypy molecule. The colloidal particles of anatase used in the experiments are characterized by a widespread and unknown distribution of the exposed surfaces. When heated, anatase spontaneously reconstructs to the more uniform rutile structure, although it is not known if and when this has happened in the experiments. The uniform 001 surface of rutile titanium dioxide is used in this simulation. It may be expected that the results obtained for the rutile surface will be characteristic of the entire class of reactions. Although experiments on this exact system have not been reported, the system is simple enough to be reproduced experimentally.

The theoretical approach used for the nonadiabatic MD simulation is described below. The theory section also introduces a straightforward criterion allowing us to separate the adiabatic and nonadiabatic contributions to an individual ET event. The simulation results are followed by summary and conclusions.

2. Theory

To carry out a nonadiabatic MD simulation, methods for calculation of electronic energy surfaces and couplings as well as for ion dynamics including nonadiabatic quantum transitions between the electronic states are required.[36−45] The semiconductor−molecule system is modeled by density functional theory (DFT),[47,48] which provides an ab initio description of both the electronic structure and ionic forces, avoiding the need for empirical MD potentials. The nonadiabatic coupling matrix elements are also calculated from the first principles, given the Kohn−Sham orbital representation of the electron density.[48] Plane wave DFT with periodic boundary conditions is the preferred method of ab initio calculations of extended systems.[49,50] DFT is able to handle simulations involving a larger number of atoms than the traditional electronic structure methods

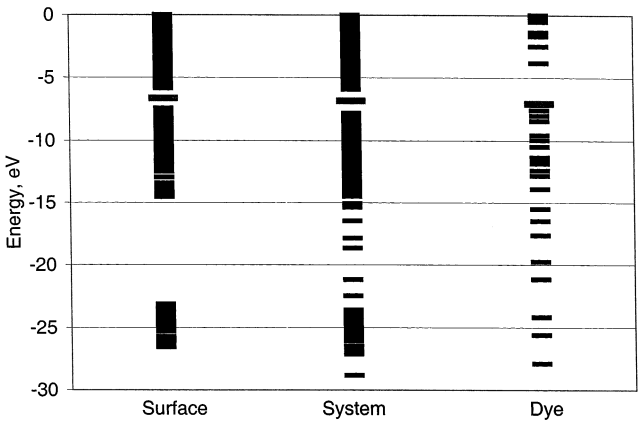

Figure 2. Kohn−Sham orbital energies of the TiO_2 surface, the isolated dye, and the combined system. The HOMO−LUMO gap of the dye equals 3.2 eV and is close to the 3.4 eV energy of the first excited-state calculated by the time-dependent DFT. The HOMO−LUMO excitation contributes about 70% to the TD-DFT excited state, indicating that the Kohn−Sham LUMO gives a good representation of the excited state. The longer gray lines represent the Fermi energy.

of comparable accuracy, for example, the second-order Möller−Plesset perturbation theory.[51] Plane wave basis sets with the associated fast Fourier transform algorithms are more efficient at representing extended systems than either cluster or embedded calculations using localized Gaussian basis sets.[52]

The DFT simulations are performed with the VASP code.[52−54] The core electrons are simulated using the Vanderbilt pseudopotentials,[55] and only the valence electrons are treated explicitly. The generalized gradient functional due to Perdew and Wang[49] is used. The Kohn−Sham orbitals are constructed from the plane wave basis set and are used to describe the electronic states of the system (Figure 2). The electronic structure of the dye has been additionally investigated by DFT in a Gaussian basis.[51] In particular, the energy gap between the ground and first excited states of the molecule has been calculated by the time-dependent (TD) DFT that is designed for the description of excited states. The TD-DFT energy gap calculated using the 6-31g* Gaussian basis set and the Perdew−Wang DFT functional equals 3.4 eV and is close to the 3.2 eV gap between the highest occupied (HOMO) and lowest unoccupied (LUMO) Kohn−Sham orbitals observed in the plane-wave DFT calculation. The TD-DFT calculation predicts that the one electron HOMO−LUMO excitation contributes around 70% to the first excited-state density. Due to this fact, the Kohn−Sham LUMO provides a good representation of the photoexcited state. A similar result holds for the next two excited states of the dye. The plane-wave DFT calculation on the combined semiconductor−dye system gives electronic states that are well localized either on the dye or in the semiconductor and correspond to the states of the isolated subsystems. This agrees with the experimental observation that the photoinduced ET occurs in a sequential manner with an initial gas-phase-like molecular excitation and a subsequent molecule−surface transfer[11,18,56] and not by a direct molecule−semiconductor photoexcitation as in catechol/TiO_2[57] and $Fe(CN)_6^{4-}/TiO_2$[58] systems.

The following simulation protocol is adopted. The initial system configuration is obtained in the standard surface calculation method. First, the geometry of a bulk TiO_2 cell is minimized to find the minimum energy configuration for the bulk within the DFT framework. Then, the size of the cell is increased and a layer of vacuum is added in one dimension (see Figure 1) making the system a periodic stack of infinite slabs. It is important to have a large enough vacuum layer that the top of one slab does not interact with the bottom of the next slab within

the infinite array of slabs. The surfaces of the slab are terminated with hydrogen atoms. The termination avoids the electron density from the broken bonds at the hedged surface extending into the vacuum, which would otherwise increase the danger of the artificial interaction between the slabs. Similar to the minimization of the bulk configuration the chromophore structure is minimized in the DFT framework. The obtained minimum energy configuration of the molecule is subsequently added to the reactive surface of the slab. The molecule is attached to the slab by mimicking a dehydration reaction between the carboxylic group of the chromophore and a hydroxyl group on the surface (see Figure 1). The top few layers of the system are allowed to relax while the bottom two layers are held fixed.

The ab initio MD simulations are performed with a 1 fs time step. The assembled structure of the dye on the TiO_2 surface is brought to the experimental temperature of 50 K during a 1 ps equilibration run using a Nose thermostat.[59] Then, a 500 fs ground-state production run is completed. Ten random configurations are harvested from the production run to use as initial configurations of the system at the time the photon is absorbed. For each configuration the Kohn−Sham orbital corresponding to the chromophore first excited state is determined. An electron from an occupied orbital is promoted to the excited-state orbital to initiate a nonadiabatic MD run. A total of 10 runs are carried out.

The nonadiabatic MD simulations are conducted by the quantum-classical mean-field (MF) approximation, where the time-dependent quantum Schrödinger equation for the electronic degrees of freedom is coupled to the classical Newton equation for the ions.[43−45,60−64] The Kohn−Sham orbitals $\phi_i(r)$ are obtained for the instantaneous values of the ionic positions $R(t)$ and form a complete basis set representing the TD electronic wave function $\Psi(r,t)$:

$$\Psi(r,t) = \sum_i c_i(t)\, \phi_i(r) \tag{1}$$

The explicit time dependence of $\Psi(r,t)$ appears in the expansion coefficients. $\Psi(r,t)$ evolves according to the TD Schrödinger equation

$$i\hbar\frac{\partial}{\partial t}\Psi(r,t) = H(r;R(t))\, \Psi(r,t) \tag{2}$$

whose Hamiltonian $H(r;R(t))$ parametrically depends on ionic coordinates $R(t)$. The TD wave function $\Psi(r,t)$ defines the quantum force F_{qm} that moves the ions:

$$F_{qm} = -\nabla_R\langle\Psi(r,t)|H(r;R)|\Psi(r,t)\rangle \tag{3}$$

The diagonal matrix elements of the Hamiltonian are given by the Kohn−Sham orbital energies. The off-diagonal nonadiabatic coupling matrix elements are calculated numerically on the basis of the overlap of the Kohn−Sham orbitals at sequential time steps according to the method of Hammes-Schiffer and Tully[36]

$$\begin{aligned} i\hbar\langle\phi_i|\nabla_R|\phi_j\rangle\cdot\dot{R} &= i\hbar\left\langle\phi_i\left|\frac{\partial}{\partial t}\right|\phi_j\right\rangle \\ &\approx \left(\frac{1}{2\Delta t}\right)(\langle\phi_i(t)|\phi_j(t+\Delta t)\rangle - \langle\phi_i(t+\Delta t)|\phi_j(t)\rangle) \end{aligned} \tag{4}$$

Note that the nonadiabatic coupling matrix element defined in eq 5 is the inner product of the electronic coupling and the ionic velocity vectors. Using the Hellmann−Feynman theorem,[65] the electronic coupling can be expressed with an explicit dependence on the electronic energy gap $E_j - E_i$

$$\langle\phi_i|\nabla_R|\phi_j\rangle = \frac{\langle\phi_i(r)|\nabla_R H(r;R)|\phi_j(r)\rangle}{E_j(R) - E_i(R)} \tag{5}$$

The numerator above defines the ET matrix element entering the standard nonadiabatic theories of ET, such as the Mulliken−Hush theory[66−69] and is weakly dependent on the electronic energy gap. The approach of Hammes-Schiffer and Tully[36] avoids direct calculation of $\langle\phi_i(r)|\nabla_R H(r;R)|\phi_j(r)\rangle$, providing a great computational advantage in the multidimensional system considered here.

The state occupations are propagated using the second order differencing scheme[70]

$$\Psi(t+\Delta t) = \Psi(t-\Delta t) - \frac{2i}{\hbar}\Delta t H\Psi(t) \tag{6}$$

that, by preserving the time symmetry, is stable and conserves both the energy and the norm of the wave function. Up to 100 states nearest in energy to the initially occupied excited state have been included in the simulation, with the majority of the nonadiabatic dynamics runs carried out using 40 states. A total of 1000 electronic steps are performed per single 1 fs MD step.

The extent of ET is determined by integration of the total excited state electron density over the region of the simulation cell occupied by the molecule, Figure 1. Though the surface dividing the reactant and product regions should be determined variationally by minimizing the flux,[71] significant flexibility in the choice of the surface exists, because the electronic excitation is localized within the π-electron system of the dye and does not extend onto the bridge or the semiconductor. Any plane parallel to TiO_2 and passing through the bridge connecting the molecule and the semiconductor is suitable for the definition of the reactant and product regions of the cell, Figure 1. The ET coordinate is defined by the fraction of the excited electron that has left the reactant region occupied by the molecule. The initial localization of the excited state electron is primarily on the dye, in agreement with the experiments.[11,18,56]

To differentiate between the adiabatic and nonadiabatic ET mechanisms the following procedure is proposed. The total electron density on the dye that defines the ET coordinate is given by the sum over states

$$\begin{aligned} \rho_{dye}(t) &= \int_{dye} dr\, |\Psi(r,t)|^2 \\ &= \sum_{i,j} c_i^*(t)\, c_j(t) \int_{dye} \phi_i^*(r)\, \phi_j(r)\, dr \end{aligned} \tag{7}$$

where the integration for each state is performed over the region of the simulation cell occupied by the dye. By the product rule, the change in the electron density, i.e., the electron current, that determines the extent of ET comes due to changes in either state occupations $c_i^*(t)\, c_j(t)$ or state localizations on the molecule $\int_{dye}\phi_i^*(r;R(t))\, \phi_j(r;R(t))\, dr$:

$$\begin{aligned} \frac{d\rho_{dye}(t)}{dt} = \sum_{i,j}\Bigg\{ &\frac{dc_i^*(t)\, c_j(t)}{dt}\int_{dye}\phi_i^*(r)\, \phi_j(r)\, dr + \\ &c_i(t)\, c_j(t)\, \frac{d\int_{dye}\phi_i^*(r;R(t))\, \phi_j(r;R(t))\, dr}{dt}\Bigg\} \end{aligned} \tag{8}$$

The first term describes the nonadiabatic transfer, and the second

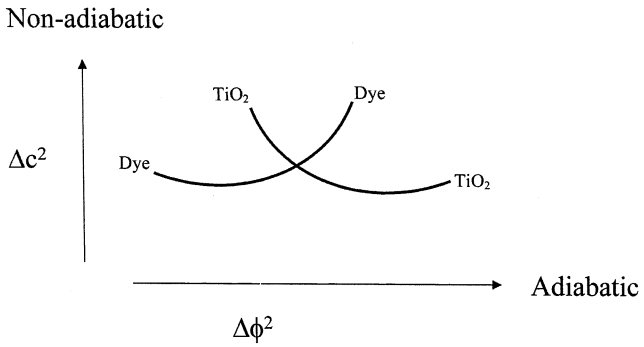

Figure 3. Adiabatic and nonadiabatic ET pathways, eq 7. ET occurs by either a change in the state occupation Δc^2, by nonadiabatic transfer, or by an adiabatic atomic motion that shifts the localization of the adiabatic state $\Delta\phi^2$ away from the dye.

term gives the adiabatic transfer, as illustrated in Figure 3. It is straightforward to keep track of the adiabatic and nonadiabatic contributions to the overall ET by integration of the two terms of (8) over time. Because the basis states are typically well localized on either the dye or the semiconductor, the off-diagonal contributions to ρ_{dye} are negligible, and simplified expressions can be used in place of eqs 7 and 8:

$$\rho_{dye}(t) = \int_{dye}|\Psi(r,t)|^2\,dr \approx \sum_i |c_i(t)|^2 \int_{dye}|\phi_i(r)|^2\,dr \quad (9)$$

$$\frac{d\rho_{dye}(t)}{dt} = \frac{d\int_{dye}|\Psi(r,t)|^2\,dr}{dt} \approx \sum_i \frac{d|c_i(t)|^2}{dt}\int_{dye}|\phi_i(r)|^2\,dr + \sum_i |c_i(t)|^2 \frac{d\int_{dye}|\phi_i(r;R(t))|^2\,dr}{dt} \quad (10)$$

The differentiation between the adiabatic and nonadiabatic ET mechanisms introduced above relies on the adiabatic representation ϕ_i of the total wave function Ψ. Only in this case do changes in the localization of ϕ_i represent purely adiabatic transfer. The nonadiabatic and adiabatic contributions to ET defined above add up to the total ET. Though the total ET is always positive, either of the contributions can become negative describing situations, where a forward ET by one mechanism is accompanied by a backward ET by the other mechanism. The proposed procedure is general and can be applied to other systems and simulation approaches that give localizations and occupations of adiabatic states.

3. Results and Discussion

The results of the simulation indicate that the photoinduced ET from a molecular donor to the semiconductor substrate involves a variety of processes. Both adiabatic and nonadiabatic ET mechanisms are present, involving localized avoided crossings and extended regions of nonadiabatic coupling. Though a continuum of states in the semiconductor is in resonance with the molecular excited state, only relatively few of them interact with the molecule and are capable of accepting the electron. In addition to being close in energy, the acceptor states must be localized on the surface near the semiconductor−dye junction. The key features of the ET process discerned in the simulation are illustrated below with sample nonadiabatic MD trajectories. The variations in both ET rates and mechanisms are great from trajectory to trajectory and deserve as much consideration as the average ET behavior, which is discussed at the end of this section.

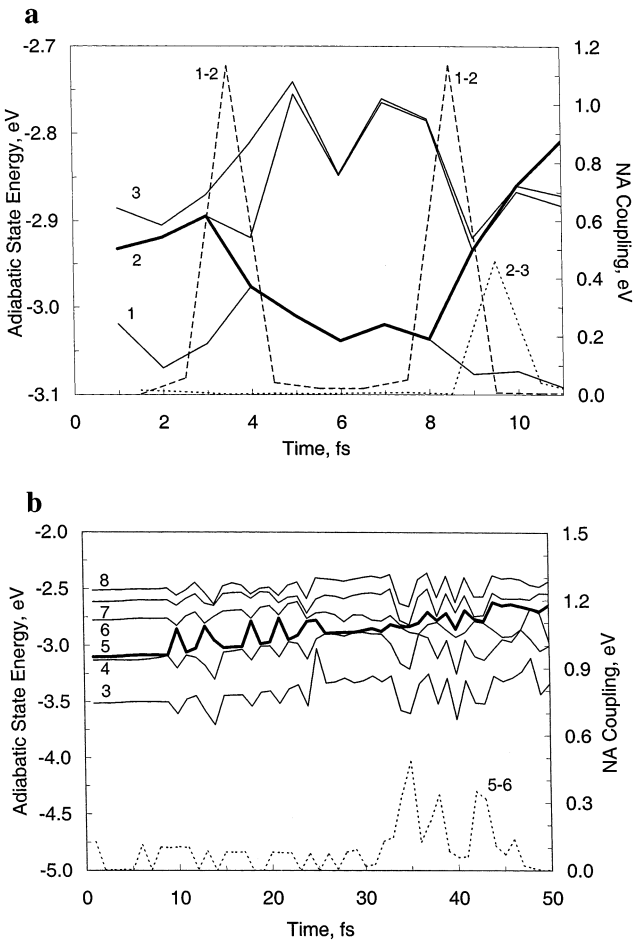

Figure 4. Typical values of the electronic state energies (solid lines) and nonadiabatic couplings (dashed and dotted lines), eq 5, representing (a) two successive localized avoided crossing regions and (b) an extended coupling region. The explicit energy dependence of the coupling is given in eq 5. The coupling in the localized regions is several times stronger than the coupling in the extended region. The bold line indicated the state with the largest occupation. The states are numbered for convenience only. In both cases a total of 40 states are included in the simulation.

Figure 4a shows part of a trajectory with two consecutive localized avoided crossing regions that result in a quantum mechanical interference effect known as a Stueckelberg oscillation.[35,43,72] The adiabatic energies and the nonadiabatic coupling matrix elements are presented for 3 of the 40 states in the simulation, including the photoexcited state. The absolute values of the nonadiabatic coupling matrix elements, eq 5, sharply peak at the avoided crossings due to the energy gap dependence, eq 5, and are essentially zero away from the crossings. Though states 2 and 3 are nearly degenerate in energy, they become coupled only at the end of this trajectory. The energy resonance is required, but not sufficient, for the interaction between the states. States 1 and 2 are not as close in energy as states 2 and 3; however, they are coupled due to a favorable spatial overlap. The localization of the states constantly changes due to ion dynamics that by the end of this sample run drives the densities of states 2 and 3 to overlap. The occupations of the states are changing as well. The largest occupation, indicated by the bold line, moves initially from state 2 to 1 and then back to 2, 3 and at the very end to state 4. Thus, the dynamics of this short 10 fs part of the trajectory is quite rich and complex.

In contrast to the nonadiabatic MD trajectory shown in Figure 4a, the electron in the trajectory of Figure 4b remains in the photoexcited state for over 30 fs. A sequence of near-

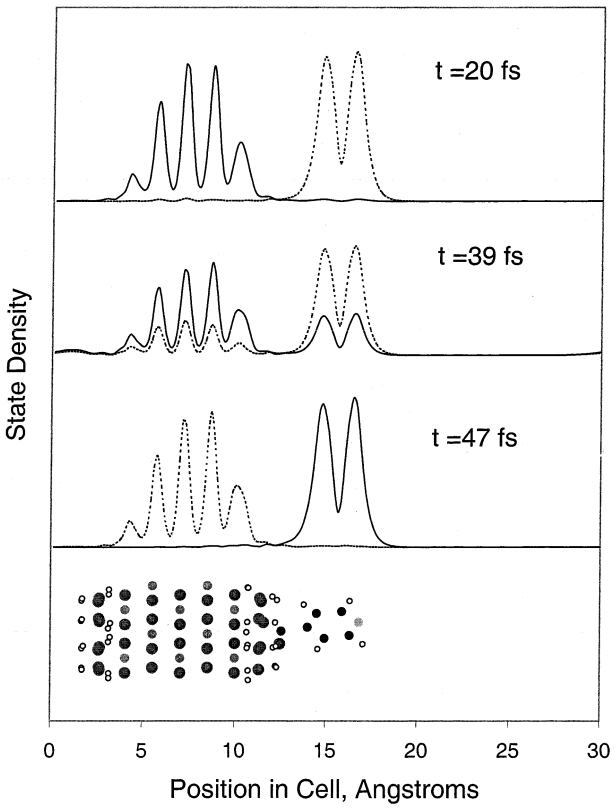

Figure 5. Evolution of the adiabatic electronic states in the extended coupling region shown in Figure 4b. The photoexcited π^* state of the dye and a TiO_2 surface state do not overlap for the first 20 fs of the evolution. Then, the states slowly mix and come out of the coupling region with the populations that depend on the strength and duration of the nonadiabatic coupling. With localized avoided crossing such as those shown in Figure 4a the adiabatic states switch instantaneously on the time scale of the MD step.

degeneracies between the initial state 5 and state 6 accompanied by small increases in the nonadiabatic coupling does result in a leakage of population from state 5 to state 6. In each of these instances state 5 remains localized on the dye and state 6 on the semiconductor. Because states 5 and 6 do not switch their diabatic character, the approaches between the states are not avoided crossings, but rather a prologue to an extended nonadiabatic coupling region. Between 30 and 50 fs the coupling becomes stronger. It can be noticed that initially the energy of the molecular state 5 oscillates out of phase with the energies of the semiconductor states. The oscillation is in phase during the second part of the trajectory. The in-phase oscillation indicates that the electron donor and acceptor states depend on the ionic coordinates in the same manner. This results in an increased nonadiabatic coupling and an ET away from the molecular state. The nonadiabatic coupling in the extended coupling region, Figure 4b, is 2−3 times weaker than that of the localized avoided crossings shown in Figure 4a, and the overall ET dynamics is an order of magnitude slower.

The evolution of the densities of the two interacting states from the extending coupling region, states 5 and 6 in Figure 4b, is illustrated in Figure 5. The photoexcited electron density is contained in the dye, and the semiconductor state that is about to mix with the molecular state extends four layers into the surface. On the 20th femtosecond of the trajectory the states are still well localized in the dye and the surface. The states reach the maximum degree of mixing around the 40th femtosecond, and in another 7 fs they are localized once again. The slow mixing and demixing of the states agrees with the extended nature of the nonadiabatic coupling of Figure 4b.

A three-dimensional view of the coupled molecular and semiconductor states is presented in Figure 6a. The π^* origin of the dye excited state can be clearly seen in the figure. The semiconductor state extends radially into the surface and away from the point of contact between the molecule and the semiconductor. The semiconductor state originates from the d orbitals of the Ti atoms, as illustrated by the projection of the semiconductor state density on the plane perpendicular to the cell's longest axis, Figure 6b. The density of the semiconductor state is delocalized over several Ti atoms in the second and third surface layers, Figure 6a. The density in the first layer is dominated by a single Ti atom. A small asymmetry in the molecular orientation with respect to the surface, Figure 1, breaks the symmetry of the density of the first surface layer most strongly. Integration of the state density in Figure 5 leads to the conclusions that the dominant Ti atom is responsible for about 20% of ET. Control of the electronic response of the solid to the electronic excitation in the molecule by a single first layer atom is similar to the domination of a single first shell solvent molecule in the short-time solvent response of a liquid to an electronic excitation in a solute.[73] In both cases the short time interaction of an extended system with a molecular system appears to be a local event. The local nature of the interaction is more pronounced in a liquid medium, as should be expected; however, the fact that 20% of the response of a periodic solid is due to a single atom is rather surprising.

Localizations, eq 9, occupations $|c_i|^2$ of the dominant states, and the adiabatic and nonadiabatic contributions to the ET coordinate, eq 10, are given in Figure 7a,b for two nonadiabatic MD trajectories. The trajectory of Figure 7a is primarily a nonadiabatic ET. It is another example of an extended nonadiabatic coupling region with a slow transfer of the electronic occupation from the molecular to a semiconductor state. Late in the trajectory an avoided crossing is encountered, producing some amount of adiabatic transfer. Involvement of several states in the transfer process is characteristic of nonadiabatic ET. In the example considered in Figure 7a, the occupations of the three dominant states rise above 20% over the duration of the run. The occupations of the remaining states are also significant and add up to another 20% by the end of the run. In contrast, a trajectory with a predominantly adiabatic ET, Figure 7b, involves only two states, with most of the transfer occurring during a short time interval of the first avoided crossing. The subsequent avoided crossings involving the photoexcited state are irrelevant, because the electron has already moved to the semiconductor and is no longer likely, by pure probability, to find the molecular state again.

The features of all 10 trajectories are summarized in Table 1. The trajectories showing primarily nonadiabatic behavior exhibit faster ET in comparison with the adiabatic ET trajectories. Adiabatic transfer requires an avoided crossing region and a strong coupling. To achieve such conditions, the system must interrogate more of its configuration space than in the case of nonadiabatic transfer, where the presence of several weakly coupled semiconductor states is sufficient. However, once an appropriate avoided crossing is located, the adiabatic transfer proceeds quickly and efficiently. In several cases both adiabatic and nonadiabatic pathways are significant and combine to result in a fast ET. Sometimes, when neither of the mechanisms is efficient, the ET is unusually slow. Trajectory 2 shows an interesting case of an adiabatic back ET that follows a nonadiabatic forward transfer. The back transfer occurred when an extended coupling region involving several states terminated in an avoided crossing between two of the states, one of them localized on the molecule. The nonadiabatic ET was partially

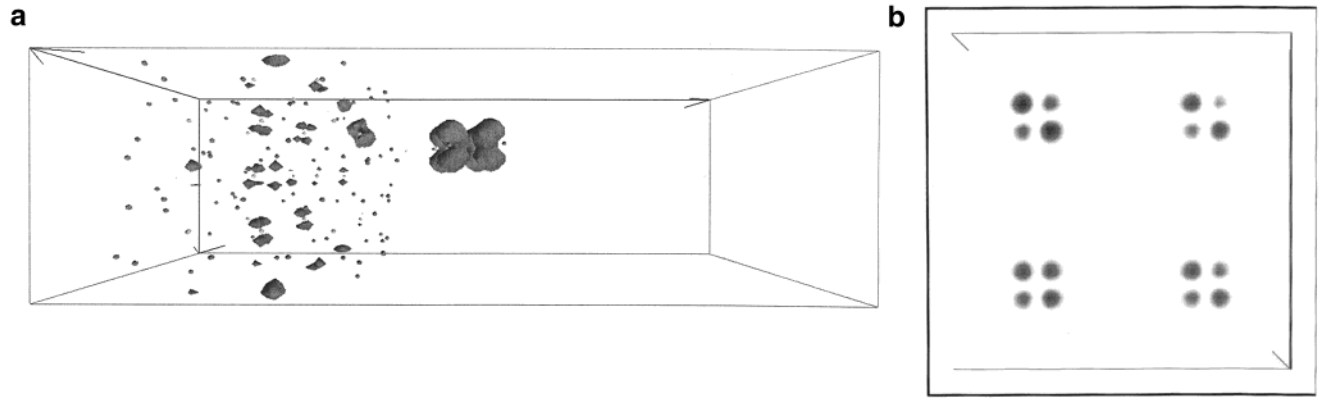

Figure 6. (a) Three-dimensional electron density of the delocalized state shown in Figure 5 by the dashed line at 39 fs. The π-electron nature of the dye excited state is clearly seen. The semiconductor state coupled to the dye state is formed by d orbitals of Ti atoms and extends four layers into the surface. (b) The d orbital origin of the semiconductor state is illustrated by a density slice taken perpendicular to the cell's longest dimension.

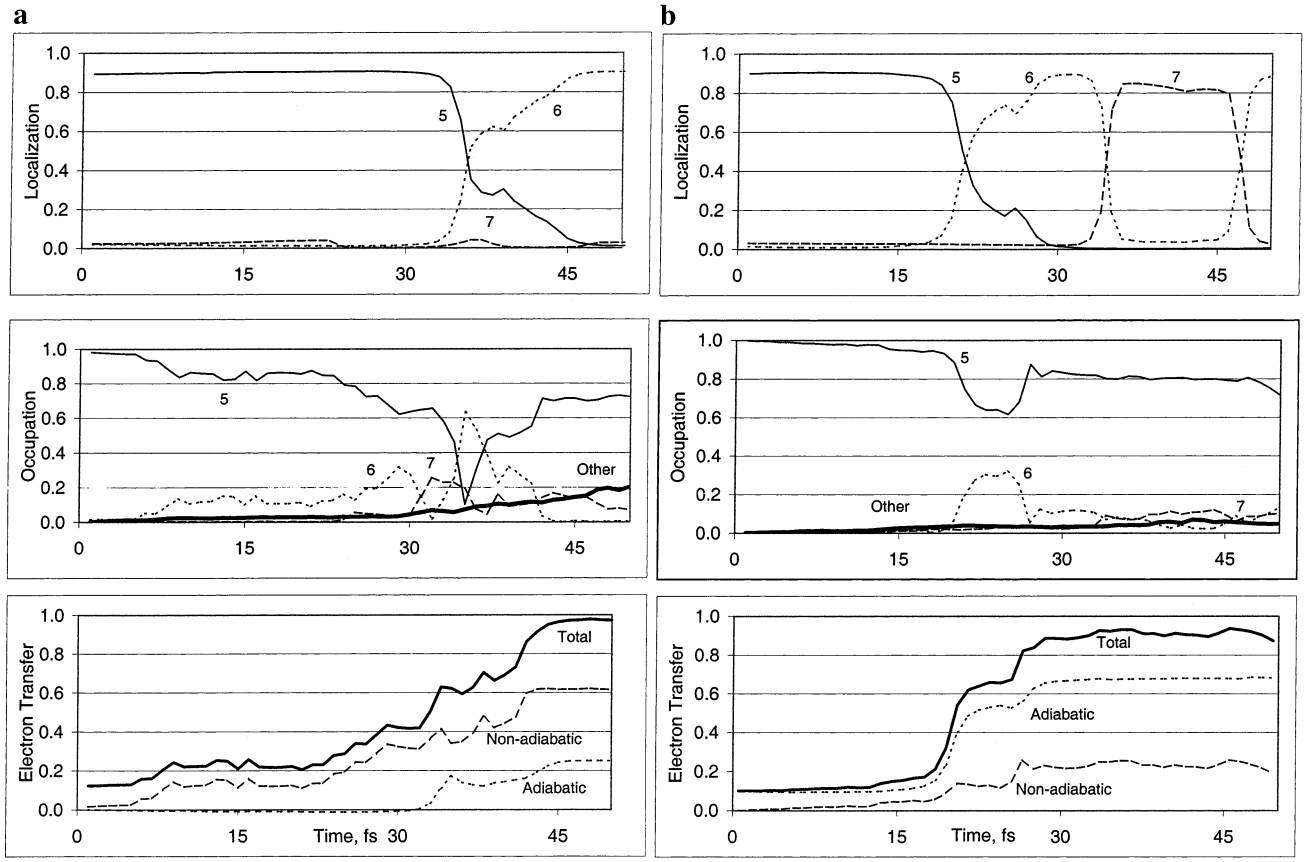

Figure 7. (a) Time evolution of state localizations, occupations, and the ET coordinate along a trajectory with primarily nonadiabatic ET. Occupation of three states reaches above 20% and the cumulative occupation of the remaining states rises to 20%. The adiabatic and nonadiabatic contributions to ET are calculated according to eq 10. (b) Same as (a), but for a predominantly adiabatic trajectory. Only two states have occupations above 20% and the cumulative occupation of the remaining states is insignificant.

adiabatically reversed by the avoided crossing interaction between the two states.

The time dependence of the ET coordinate averaged over the 10 nonadiabatic MD runs is presented in Figure 8, together with the averaged nonadiabatic and adiabatic contributions to the overall ET. The data are fitted by an exponential

$$\mathrm{ET} = (1 - \mathrm{e}^{t/\tau})C \qquad (11)$$

The constant C equals 1 for the total transfer and 0.56 and 0.44 for the nonadiabatic and adiabatic contributions, respectively. The 28 fs ET time scale falls on the fast side of the range of the experimental observations made for a variety of chromophores. The fastest observed ET time scale is less than the instrument response time of 25 fs,[18] whereas the slower ET events observed with the TiO_2 substrate extend for several hundred femtoseconds.[11,14−16] A tight-binding model calculation of the electron injection time across the metaloxide-molecule interface gave an ET time of less than 10 fs.[30] The relatively fast ET time scale observed in our simulation is appropriate, because the chromophore is attached directly to the semiconductor without any bridge, whereas in the majority of the experiments chromophores are attached to the semiconductor via alkane bridges that decrease the donor−acceptor coupling.

The decomposition of the total ET into the nonadiabatic and adiabatic contributions shows that both pathways are about

TABLE 1: Summary of the Nonadiabatic MD Runs[a]

trajectory	adiabatic	nonadiabatic	states	time scale
1	19%	79%	6	quick (10 fs)
2	−49%[a,b]	146%	5	quick (8 fs)
3	40%	57%	4	quick (7 fs)
4	58%	27%	2	quick (12 fs)
5	69%	−10%	3	slow (33 fs)
6	71%	−09%	2	slow (137 fs)
7	28%	69%	3	slow (46 fs)
8	70%	16%	3	slow (28 fs)
9	22%	17%	2	slow (96 fs)
10	27%	58%	2	slow (36 fs)

[a] The adiabatic and nonadiabatic contributions to ET, the number of states with significant occupations and the ET time scale are shown. Generally, nonadiabatic ET proceeds faster and involves more states than adiabatic ET. [b] A strong nonadiabatic ET is followed by a partial back-ET by the adiabatic mechanism.

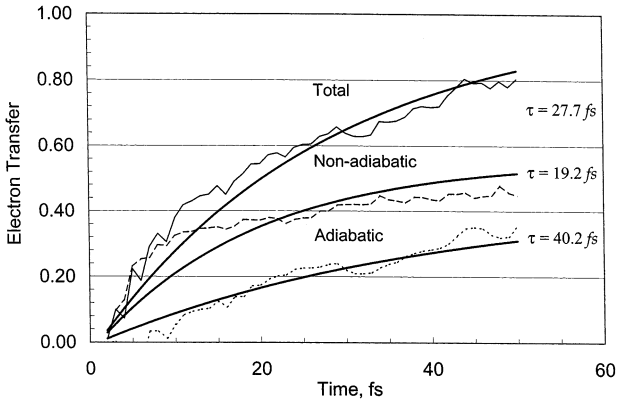

Figure 8. Time evolution of the ET coordinate averaged over 10 runs (solid line) is split into the adiabatic (dotted line) and nonadiabatic (dashed line) contributions according to eq 10. Exponential fits to the data are given by the thick lines. The adiabatic transfer is slower than the nonadiabatic transfer. However, the nonadiabatic mechanism is not always available, depending on the instantaneous ionic configuration.

equally significant. The nonadiabatic pathway dominates at early times, whereas the adiabatic mechanism is more efficient on a slower time scale. The time scale of adiabatic transfer is determined by the time scales of the ionic motions that lead to the avoided crossing events. Because the nonadiabatic transfer proceeds very fast initially, but subsequently slows down, it may be expected that in the absence of the adiabatic mechanism, a purely nonadiabatic transfer will take a long time to finish. The single exponential fits to the simulation data are rather poor, especially for the nonadiabatic ET. The nonexponential nature of the ET process in the systems of this type is predicted by the transition state theory.[23,24]

The following general picture of the ET process has emerged. The nonadiabatic pathway is always present and contributes to the overall ET immediately following the photoexcitation. The efficiency of the nonadiabatic transfer depends on the number of semiconductor states that are localized close to the molecular state both in space and energy. The adiabatic pathway is more sensitive to the ET conditions. Adiabatic transfer is usually slow and is observed when the nonadiabatic transfer efficiency is reduced. Because the nonadiabatic pathway is determined by the weakly coupled states and the adiabatic pathway relies on the avoided crossings, the two pathways are largely independent, and a significant variation in the ET times is observed between individual ET events.

4. Discussion and Conclusions

The real-time ultrafast dynamics of the photoinduced ET process occurring between an organic sensitizer molecule and a semiconductor surface have been simulated at the atomic level. The model used in the simulation exhibits the salient features of the larger systems studied experimentally and provides a detailed picture of the ET mechanism.

The simulated ET takes place on the 30 fs time scale on the average but shows a substantial, more than an order of magnitude variation in the time scales of individual ET events. Both adiabatic and nonadiabatic mechanisms are available for the ET. Initially, the nonadiabatic pathway dominates, and the adiabatic pathway is typically nonexistent. Subsequently, the probability of the adiabatic pathway increases and competes with the nonadiabatic contribution. The adiabatic transfer involves a preliminary search for an avoided crossing region that can be located only by ionic motion. Hence, the time scale of adiabatic transfer is closely related to the time scales of the available molecular and surface modes. The identification of the modes the are most efficient promoters[74,75] of the adiabatic ET is work in progress.

The nonadiabatic ET mechanism relies on a weaker coupling of the molecular state to a few states of the semiconductor and can occur either near avoided crossing or in extended regions of nonadiabatic coupling. The electron acceptor states in the semiconductor are close to the molecular state in both energy and spatial localization. Out of the continuum of the conductance band states of the semiconductor there are typically several that satisfy these requirements and are capable of nonadiabatic ET. In contrast to the adiabatic ET, the nonadiabatic ET does not require a search for an avoided crossing and starts immediately upon the photoexcitation. Whereas the nonadiabatic mechanism dominates at early times, subsequently the nonadiabatic and adiabatic contributions to the overall ET become nearly equivalent.

The photoexcited π-electron molecular state couples to the conductance band states formed by the d-electrons of the Ti atoms. The electron acceptor states that accommodate the photoexcited electron directly from the molecule typically extend three to four layers into the semiconductor surface. Rather surprisingly for a periodic solid, the initial electron acceptor states can be significantly localized on a single Ti atom in the first surface layer.

It is assumed in the simulation that the Kohn−Sham orbitals provide a reasonable adiabatic representation for the electronic states of the system. The adiabatic assumption simplifies the calculation of the off-diagonal elements of the Hamiltonian, eq 5. The nonadiabatic MD calculations can be carried out in any representation, adiabatic or any of the diabatic representations. The Kohn−Sham orbitals can be viewed simply as a convenient representation to perform the simulation. With the availability of better Hamiltonians, for instance, as in TD-DFT, corrections to the diagonal and off-diagonal elements of the Kohn−Sham representation can be introduced, and appropriate superpositions of Kohn−Sham states will represent excited states. It may be expected that such corrections will be small for the system under study, because the Kohn−Sham HOMO−LUMO gap provides a good estimate of the dye excited-state energy, and the orbitals give a good description of the more accurate TD-DFT excited-state densities.

The simulations have been performed by a mixed quantum-classical mean-field approach that neglects the quantum effects of the ionic motion, in particular, zero point energy (ZPE) and decoherence effects.[64,76−80] ZPE increases the ionic kinetic energy entering the nonadiabatic coupling matrix element, eq 5, and, therefore, accelerates nonadiabatic ET.[78] Generally, quantum decoherence can be expected to slow nonadiabatic

transitions,[64,76,77,79] although cases are known where decoherence accelerates transitions by randomization of quantum populations.[81] The adiabatic ET is not affected by electronic decoherence, because it proceeds in the same electronic state. Similar to nonadiabatic transfer, adiabatic dynamics is accelerated by the excess kinetic energy of zero point motion. The quantum mechanics of atomic modes can be incorporated into the simulation by the recently proposed extensions of the quantum-classical mean-field method, namely, stochastic mean-field for decoherence[44] and quantized mean-field for ZPE.[45]

Acknowledgment. The financial support of NSF, CAREER Award CHE-0094012, is gratefully acknowledged. O.V.P. is a Camille and Henry Dreyfus New Faculty and an Alfred P. Sloan Fellow.

References and Notes

(1) Ferrere, S.; Gregg, B. *J. Phys. Chem. B* **2001**, *105*, 7602.
(2) Kisch, H.; Lindner, W. *Chem. Z.* **2001**, *35*, 250.
(3) Licht, S.; Wang, B.; Mukerji, S.; Soga, T.; Umeno, M.; Tributsch, H. *Int. J. Hydrogen Energy* **2001**, *26*, 653.
(4) Nozik, A. J.; Memming, R. *J. Phys. Chem.* **1996**, *100*, 13061−13078.
(5) Kamat, P. V.; Meisel, D. *Semiconductor Nanoclusters − Physical, Chemical, and Catalytic Aspects*; Elsevier: Amsterdam, 1997; Vol. 103.
(6) Schwarz, O.; van Loyen, D.; Jockusch, S.; Turro, N. J.; Duerr, H. *J. Photochem. Photobiol. A: Chem.* **2000**, *132*, 91.
(7) Oregan, B.; Grätzel, M. *Nature* **1991**, *353*, 6346.
(8) Ellingson, R. J.; Asbury, J. B.; Ferrere, S.; Ghosh, H. N.; Sprague, J. R.; Lian, T.; Nozik, A. J. *J. Phys. Chem. B* **1998**, *102*, 6455.
(9) Huang, S. Y.; Schlichthörl, G.; Nozik, A. J.; Grätzel, M.; Frank, A. J. *J. Phys. Chem. B* **1997**, *101*, 2576−2582.
(10) Tachibana, Y.; Moser, J. E.; Grätzel, M.; Klug, D. R.; Durrant, J. R. *J. Phys. Chem. B* **1996**, *100*, 20056.
(11) Asbury, J. B.; Hao, E.; Wang, Y.; Ghosh, H. N.; Lian, T. *J. Phys. Chem. B* **2001**, *105*, 4545−4557.
(12) Kelly, C. A.; Meyer, G. J. *Coord. Chem. Rev.* **2001**, *211*, 295−315.
(13) Heimer, T. A.; Heilweil, E. J. *J. Phys. Chem. B* **1997**, *101*, 10990.
(14) Willig, F.; Zimmermann, C.; Ramakrishna, S.; Storck, W. *Electrochim. Acta* **2000**, *45*, 4565−4575.
(15) Asbury, J. B.; Hao, E.; Wang, Y.; Ghosh, H. N.; Lian, T. *J. Phys. Chem. B* **2001**, *105*, 4545.
(16) Huber, R.; Spoerlein, S.; Moser, J. E.; Graetzel, M.; Wachtveitl, J. *J. Phys. Chem. B* **2000**, *104*, 8995.
(17) Asbury, J. B.; Ellingson, R. J.; Ghosh, H. N.; Nozik, A. J.; Ferrere, S.; Lian, T. *J. Phys. Chem. B* **1999**, *103*, 3110.
(18) Hannappel, T.; Burfeindt, B.; Storck, W.; Willig, F. *J. Phys. Chem. B* **1997**, *101*, 6799.
(19) Marcus, R. A. *J. Chem. Phys.* **1965**, *43*, 679.
(20) Levich, V. G.; Dogonadze, R. R. *Dokl. Akad. Nauk SSSR* **1959**, *124*, 123.
(21) Bixon, M.; Jortner, J. *J. Chem. Phys.* **1968**, *48*, 715.
(22) Gerischer, H. *Z. Phys. Chem. Frankfurt* **1961**, *27*, 48.
(23) Gao, Y. Q.; Georgievskii, Y.; Marcus, R. A. *J. Chem. Phys.* **2000**, *112*, 3358−3369.
(24) Gosavi, S.; Marcus, R. A. *J. Phys. Chem. B* **2000**, *104*, 2067−2072.
(25) Bixon, M.; Jortner, J. *Adv. Chem. Phys.* **1999**, *106*, 35.
(26) Boroda, Y. G.; Voth, G. A. *J. Electroanal. Chem.* **1998**, *450*, 95−107.
(27) Calhoun, A.; Voth, G. A. *J. Phys. Chem. B* **1998**, *102*, 8563−8568.
(28) Matyushov, D. V.; Voth, G. A. *J. Chem. Phys.* **2000**, *113*, 5413−5424.
(29) Yaliraki, S. N.; Roitberg, A. E.; Gonzales, C.; Mujica, V.; Ratner, M. A. *J. Chem. Phys.* **1999**, *111*, 6997−7002.
(30) Petersson, A.; Ratner, M.; Karlsson, H. O. *J. Phys. Chem. B* **2000**, *104*, 8498−8502.
(31) Mujica, V.; Ratner, M. A. *Chem. Phys.* **2001**, *264*, 365−370.
(32) Smith, B. B.; Nozik, A. J. *J. Phys. Chem. B* **1997**, *101*, 2459−2475.
(33) Smith, B. B.; Nozik, A. J. *J. Phys. Chem. B* **1999**, *103*, 9915−9932.
(34) Tully, J. C.; Preston, R. K. *J. Chem. Phys.* **1971**, *55*, 562.
(35) Tully, J. C. *J. Chem. Phys.* **1990**, *93*, 1061.
(36) Hammes-Schiffer, S.; Tully, J. C. *J. Chem. Phys.* **1994**, *101*, 4657.
(37) Tully, J. C. In *Classical and Quantum Dynamics in Condensed Phase Simulations*; Berne, B. J., Ciccotti, G., Coker, D. F., Eds.; World Scientific: Singapore, 1998.
(38) Sun, X.; Miller, W. H. *J. Chem. Phys.* **1997**, *106*, 6346.
(39) Volobuev, Y. L.; Hack, M. D.; Topaler, M. S.; Truhlar, D. G. *J. Chem. Phys.* **2000**, *112*, 9716.
(40) Coker, D. F. In *Computer Simulations in Chemical Physics*; Allen, M. P., Tildesley, D. J., Eds.; Kluwer Academic Publishers: Netherlands, 1993.
(41) Herman, M. F. *Annu. Rev. Phys. Chem.* **1994**, *45*, 83.
(42) Webster, F. A.; Rossky, P. J.; Friesner, R. A. *Comput. Phys. Commun.* **1991**, *63*, 494.
(43) Prezhdo, O. V.; Rossky, P. J. *J. Chem. Phys.* **1997**, *107*, 825.
(44) Prezhdo, O. V. *J. Chem. Phys.* **1999**, *111*, 8366.
(45) Brooksby, C.; Prezhdo, O. V. *Chem. Phys. Lett.* **2001**, *346*, 463−469.
(46) Burfeindt, B.; Hannappel, T.; Storck, W.; Willig, F. *J. Phys. Chem. B* **1996**, *100*, 16463.
(47) Hohenberg, P.; Kohn, W. *Phys. Rev.* **1964**, *136*, B864.
(48) Kohn, W.; Sham, L. J. *Phys. Rev.* **1965**, *140*, A1133.
(49) Perdew, J. P. In *Electronic Structure of Solids*; Ziesche, P., Eschrig, H., Eds.; Akademie Verlag: Berlin, 1991.
(50) Kohn, W.; Becke, A. D.; Parr, R. G. *J. Phys. Chem.* **1996**, *100*, 12974.
(51) Frisch, M. J.; Trucks, G. W.; Schlegel, H. B.; Scuseria, G. E.; Robb, M. A.; Cheeseman, J. R.; Zakrzewski, V. G.; Montgomery, J. A., Jr.; Stratmann, R. E.; Burant, J. C.; Dapprich, S.; Millam, J. M.; Daniels, A. D.; Kudin, K. N.; Strain, M. C.; Farkas, O.; Tomasi, J.; Barone, V.; Cossi, M.; Cammi, R.; Mennucci, B.; Pomelli, C.; Adamo, C.; Clifford, S.; Ochterski, J.; Petersson, G. A.; Ayala, P. Y.; Cui, Q.; Morokuma, K.; Malick, D. K.; Rabuck, A. D.; Raghavachari, K.; Foresman, J. B.; Cioslowski, J.; Ortiz, J. V.; Stefanov, B. B.; Liu, G.; Liashenko, A.; Piskorz, P.; Komaromi, I.; Gomperts, R.; Martin, R. L.; Fox, D. J.; Keith, T.; Al-Laham, M. A.; Peng, C. Y.; Nanayakkara, A.; Gonzalez, C.; Challacombe, M.; Gill, P. M. W.; Johnson, B. G.; Chen, W.; Wong, M. W.; Andres, J. L.; Head-Gordon, M.; Replogle, E. S.; Pople, J. A. *Gaussian 98*, revision x.x; Gaussian, Inc.: Pittsburgh, PA, 1998.
(52) Kresse, G.; Furthmüller, J. *Phys. Rev. B* **1996**, *54*, 11169.
(53) Kresse, G.; Hafner, J. *Phys. Rev. B* **1994**, *49*, 14251.
(54) Kresse, G.; Furthmüller, J. *Comput. Mater. Sci.* **1996**, *6*, 16.
(55) Vanderbilt, D. *Phys. Rev. B* **1990**, *41*, 7892.
(56) Vinodgopal, K.; Hua, X.; Dahlgren, R. L.; Lappin, A. G.; Patterson, L. K.; Kamat, P. V. *J. Phys. Chem.* **1995**, *99*, 10883−10889.
(57) Liu, Y.; Dadap, J. I.; Zimdars, D.; Eisenthal, K. B. *J. Phys. Chem. B* **1999**, *103*, 2480.
(58) Weng, Y.-X.; Wang, Y.-Q.; Asbury, J. B.; Ghosh, H. N.; Lian, T. *J. Phys. Chem. B* **2000**, *104*, 93−104.
(59) *Computer Simulations in Chemical Physics*; Allen, M. P., Tildesley, D. J., Eds.; Kluwer Academic Publishers: Netherlands, 1993.
(60) McLachlan, A. D.; Gregory, R. D.; Ball, M. A. *Mol. Phys.* **1963−64**, *7*, 119.
(61) Gerber, R. B.; Buch, V.; Ratner, M. A. *J. Chem. Phys.* **1982**, *77*, 3022.
(62) Billing, G. D. *Int. Rev. Phys. Chem.* **1994**, *13*, 309.
(63) Prezhdo, O. V.; Kisil, V. V. *Phys. Rev. A* **1997**, *56*, 162.
(64) Prezhdo, O. V.; Brooksby, C. *Phys. Rev. Lett.* **2001**, *86*, 3215.
(65) Epstein, S. T. In *Force Concept in Chemistry*; Van Nostrand Reinhold: New York, 1981.
(66) Hush, N. S. *Trans. Faraday Soc.* **1961**, *57*, 557.
(67) Hush, N. S. *Electrochim. Acta* **1968**, *13*, 1005.
(68) Cave, R. J.; Newton, M. D. *Chem. Phys. Lett.* **1996**, *249*, 15.
(69) Prezhdo, O. V.; Kindt, J. T.; Tully, J. C. *J. Chem. Phys.* **1999**, *111*, 7818.
(70) Leforestier, C.; Bisseling, R. H.; Cerjan, C.; Feit, M. D.; Friesner, R.; Guldberg, A.; Hammerich, A.; Jolicard, G.; Karrlein, W.; Meyer, H. D.; Lipkin, N.; Roncero, O.; Kosloff, R. *J. Comput. Phys.* **1991**, *94*, 59−80.
(71) Truhlar, D. G.; Garrett, B. C.; Klippenstein, S. J. *J. Phys. Chem.* **1996**, *100*, 12771.
(72) Nikitin, E. E. *Theory of Elementary Atomic and Molecular Processes in Gases*; Clarendon: Oxford, U.K., 1974.
(73) Tran, V.; Schwartz, B. J. *J. Phys. Chem. B* **1999**, *103*, 5570−5580.
(74) Prezhdo, O. V.; Rossky, P. J. *J. Phys. Chem.* **1996**, *100*, 17094.
(75) Mosyak, A. A.; Prezhdo, O. V.; Rossky, P. J. *J. Mol. Struct.* **1999**, *485−486*, 545.
(76) Bittner, E. R.; Rossky, P. J. *J. Chem. Phys.* **1995**, *103*, 8130.
(77) Schwartz, B. J.; Bittner, E. R.; Prezhdo, O. V.; Rossky, P. J. *J. Chem. Phys.* **1996**, *104*, 5942.
(78) Prezhdo, O. V.; Rossky, P. J. *J. Chem. Phys.* **1997**, *107*, 5863.
(79) Prezhdo, O. V.; Rossky, P. J. *Phys. Rev. Lett.* **1998**, *81*, 5294.
(80) Prezhdo, O. V.; Pereverzev, Y. V. *J. Chem. Phys.* **2000**, *113*, 6557.
(81) Prezhdo, O. V. *Phys. Rev. Lett.* **2000**, *85*, 4413.